Hypersingular integral-equation solution for a finite-draft surface-piercing cylindrical shell at high- and low-frequency

Ronald W. Yeung* and Mohamed Hariri Nokob†
Department of Mechanical Engineering
University of California at Berkeley
Berkeley, CA 94720-1740, USA
* Correspondence author: rwyeung@berkeley.edu
† Presenter: mhariri@berkeley.edu

1. Background

A monocolumn structure, with a circular moonpool and internal dock to act as a so-called HUB, is considered as an intermediate station for transporting people to offshore locations in the Santos Oilfield in Brazil [1]. Such designs are promising and considered to be built. A split opening in the design allows marine vehicles in and out, thus acting as a floating harbor. In this work, we present a simplified model of such a harbor and develop the numerics to analyze the problem eventually. The body S considered is a floating bottomless harbor of circular cylindrical shape of radius a and draft d floating in deep water (see Fig.1). Modeling of similar problems using eigen-function expansion method (EEM) gained interest in the 80's (see, e.g. Yeung [2]).

We consider a general point $P=(x,y,z)$ in the fluid domain and another point $Q=(\xi,\eta,\zeta)$ on the surface of S. The coordinate system is taken to be on the still free surface with the y axis pointing upwards. We can state the "standard" problem as follows:

$$\nabla^2\phi = 0 \tag{1}$$

$$\phi_y - \nu\phi = 0,\ y = 0;\quad \nabla\phi = 0,\ y \to -\infty \tag{2}$$

$$\phi_n = \vec{V} \bullet \vec{n}(P),\ \vec{V} = (U_1, 0, U_2),\quad \text{for } P \text{ on } S \tag{3}$$

Here, the velocity potential is $\Phi = \mathrm{Re}\{\phi e^{-i\omega t}\}$ and (U_1, U_2) are the surge and sway velocities of S. The frequency factor $\nu = \omega^2/g$ is either zero or infinite in this work. The thickness of the boundary wall is infinitely thin and accordingly, special treatment is required as compared to bodies of finite thickness. The BIM is known to have difficulties dealing with this kind of problems. Hence we will use a special formulation for such thin-body geometry. The general integral equation over a three dimensional environment is given by:

$$4\pi\phi(P) = -\iint_S \phi(Q)\frac{\partial G(P,Q)}{\partial n_Q} - G(P,Q)\frac{\partial \phi(Q)}{\partial n_Q} dS_Q \tag{4}$$

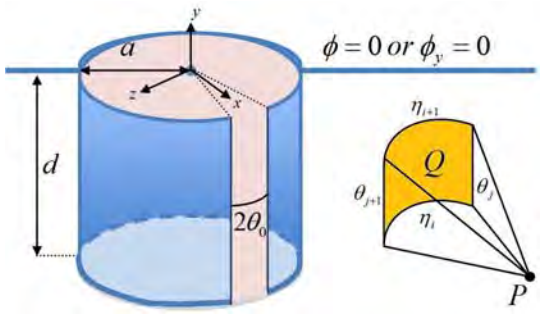

Figure 1: Sketch of the shell S and an arc-surface panel

where G is a suitable Green's function. In this work, we consider the following form of G:

$$G = \frac{1}{r_1} \pm \frac{1}{r_2} + H \tag{5}$$

$$r_{1,2} = \sqrt{(x-\xi)^2 + (y \mp \eta)^2 + (z-\varsigma)^2} \tag{6}$$

The $+(-)$ sign in (5) is chosen if the zero- (or infinite-) frequency case is considered. r_1 and r_2 correspond to the usual singular source and image reflection about $y=0$, respectively. We take $H=0$ here as it is regular when $P \to Q$ and can be handled relatively easily compared with the singular term r_1. For the thin shell case, only the dipole term remains, thus (4) reduces to

$$4\pi\phi(P) = -\iint_S [\phi(Q)]\frac{\partial G(P,Q)}{\partial n_Q} dS_Q \tag{7}$$

Here, $[\phi(Q)] \equiv \phi(a^+) - \phi(a^-)$ is the jump of ϕ across S and the integration is over the outside S only. Differentiation of (7) in the normal direction gives:

$$4\pi\frac{\partial\phi(P)}{\partial n_P} = \frac{-\partial}{\partial n_P}\iint_S [\phi(Q)]\frac{\partial\, G(P,Q)}{\partial n_Q} dS_Q \tag{8}$$

In (8), this normal velocity is explicitly given by (3) with a highly singular kernel. Only one function ϕ is present in this formulation. In fact, ϕ is proportional to the pressure difference across S and its solution is sufficient to compute the forces acting on the body.

The derivative in (8) can be taken under the integral sign on the condition that the integral be interpreted as a Hadamard finite part integral [3][4]. These integrals are usually difficult to compute and cannot be treated using standard quadrature method. The safest way to deal with them is by analytical integration when possible. This is the case in [5] and [6] for a flat surface (contour). The integral can also be treated by a process of regularization where the equation is written in terms of the unknown and its tangential derivative [3]. This procedure reduces the singularity of the integrand but leads to tangential derivatives, which are not needed for the problem and suffer from their own computational errors. By some transformations and Fourier expansions, the authors in [7] were successful in transforming the hypersingular equation to a one dimensional standard integral equation for the case of a flat disc. In this work, we tackle the problem hypersingularity using a combination of analytical integration and singularity separation.

2. Analytical Integration of the Kernel

The crux of the issue is to be able to evaluate the singular integrand of the integral equation (8):

$$\int_{\theta_0}^{2\pi-\theta_0}\int_{-d}^{0} a[\phi(Q)]\frac{\partial^2 1/r}{\partial n_P \partial n_Q}\,d\eta d\theta \qquad (9)$$

This applies for both r_1 and r_2 in (5). In practice, this integral will be discretized and only the integral over a circular-arc panel quad of $(\eta_i,\eta_{i+1},\theta_j,\theta_{j+1})$ is needed, where *i* and *j* denote the vertical and circumferential grid index (Fig. 1). The potential jump is assumed constant over each panel. The normal to the solid boundary in this case is given by:

$$\vec{n} = [\cos\theta, 0, \sin\theta] \qquad (10)$$

on the outer side and the negative of that on the inner side. Defining α so that over the surface of the body $[x,z] = a[\cos\alpha, \sin\alpha]$ and noting that $[\xi,\zeta] = a[\cos\theta, \sin\theta]$, we get, with some effort:

$$\frac{\partial^2 1/r}{\partial n_P \partial n_Q} = \frac{\cos\delta}{(2a^2(1-\cos\delta)+K^2)^{3/2}} + \frac{3a^2(1-\cos\delta)^2}{(2a^2(1-\cos\delta)+K^2)^{5/2}} \qquad (11)$$

with the definitions $\delta = \theta - \alpha$ and $K = \eta \pm y$ depending on whether r_1 or r_2 is used. The integration limits K_i and δ_j are defined in an obvious manner. Analytical integration in the vertical direction over the panel surface leads to:

$$\left[\frac{K}{2a^2(1-\cos\delta)\sqrt{2a^2(1-\cos\delta)+K^2}} + \frac{K(1-\cos\delta)}{2(2a^2(1-\cos\delta)+K^2)^{3/2}}\right]_{K_i}^{K_{i+1}} \qquad (12)$$

The case when $\delta = 0$ has a different result but is insignificant for the final evaluation. The expression of (12) has to be integrated circumferentially next over δ on the panel. The second term integral is regular with no singular points and can be integrated numerically with ease. The first integral is singular at *δ=0*. Using trigonometric identity, we can write the $\delta-$integral as:

$$\int_{\delta_j}^{\delta_{j+1}} \frac{1}{4a^2\sin^2\frac{\delta}{2}}\left[\frac{K}{\sqrt{4a^2\sin^2\frac{\delta}{2}+K^2}}\right]_{K_i}^{K_{i+1}} d\delta \qquad (13)$$

Three cases arise: $K_i < K_{i+1} < 0$, $0 < K_i < K_{i+1}$, and $K_i < 0 < K_{i+1}$. The first 2 cases are treated the same way and the integral (13) is made regular as follows:

$$\pm\int_{\delta_j}^{\delta_{j+1}} \frac{1}{4a^2\sin^2\frac{\delta}{2}}\Big(f(\delta,K_{i+1}) - f(\delta,K_i)\Big)d\delta \qquad (14)$$

$$f(\delta,K) = \frac{|K| - \sqrt{4a^2\sin^2\frac{\delta}{2}+|K|^2}}{\sqrt{4a^2\sin^2\frac{\delta}{2}+|K|^2}} \qquad (15)$$

The + (−) sign in (14) is used for the first (second) case. The absolute values are merely enforced to make the correct Taylor series expansion in what follows. The fact that this integral is *regular* can be better seen from its Taylor series near $\delta = 0$:

$$\frac{f(\delta,K)}{4a^2\sin^2\frac{\delta}{2}} = \frac{1-\sqrt{4S+1}}{4K^2S\sqrt{4S+1}} = \frac{1-3S+10S^2-35S^3}{2K^2} + O\left(\frac{S^4}{K^2}\right) \qquad (16)$$

with $S \equiv \left(a^2\sin^2\frac{\delta}{2}\right)\Big/K^2$. (17)

This expansion can also be used for the numerical integration when variable S is sufficiently small (<0.01). For the third case ($K_i < 0 < K_{i+1}$), (13) becomes:

$$\int_{\delta_j}^{\delta_{j+1}} \frac{1}{4a^2\sin^2\frac{\delta}{2}}\Big(f(\delta,K_{i+1}) + f(\delta,K_i)\Big)\,d\delta + \int_{\delta_j}^{\delta_{j+1}} \frac{1}{2a^2\sin^2\frac{\delta}{2}}d\delta \qquad (18)$$

The second integral in (18) is indeed the singular part and can be integrated analytically as follows:

$$\int_{\delta_j}^{\delta_{j+1}} \frac{1}{2a^2\sin^2\frac{\delta}{2}}d\delta = -\frac{1}{a^2}\left(\cot\frac{\delta_{j+1}}{2} - \cot\frac{\delta_j}{2}\right) \qquad (19)$$

while the first integral is regular as for the previous cases.

In this work, we are mainly interested in the added mass of the body. That is given by (surge and sway alike). In the present notations:

$$\mu_{11} = \frac{M_{11}}{2\rho\pi a^2 d}$$

$$= \frac{1}{2\pi a^2 d U_1} \int_{\theta_0}^{2\pi-\theta_0} \int_{-d}^{0} a[\phi_1(Q)]\cos\theta d\eta d\theta \qquad (20)$$

$$= \frac{1}{2\pi a d U_1} \sum_{j=0}^{N_2} \sum_{i=0}^{N_1} [\phi_1(Q)]_{ij} \cos\theta_j \Delta\eta \Delta\theta$$

Here ρ is the fluid density. The case for roll and pitch is very similar and the results are expected to be so as well and thus will not be shown here for brevity.

3. Computational Results

The hypersingular integral(-equatiuon) method (HIM) is verified by comparing the results to those from an alternative treatment using an eigenfunction expansion method that follows the work of [8]. Unlike the case of [2] or [8], there is a significant increase in the number of unknowns with the open slit, since the vertical and circumferential eigenfunctions are fully coupled. A circumferential uniform grid is used for the HIM, as this will allow the use of rules of repetition to allow efficient computations of the influence coefficients of the integral equation (8). In fact, a grid with a cosine distribution was found to produce only a slight improvement. The EEM coded was designed for finite water depth and finite frequency, while ideally, for comparison, we would like to use a method designed for infinite depth. Nevertheless, by taking the frequency of the EEM code very low and very large, the limiting behavior of the potentials can be obtained. Naturally, numerical difficulties result in these extreme frequency limits and we only expect the EEM results to be sufficiently close to the real solutions. The HIM has the advantage that a geometry with a slit opening requires the same computation time as for the closed body, contrary to the EEM which suffers from long computation times with an open body because of the large number of modal functions required for convergence.

Table 1 (page 4) shows the surge added-mass results for the closed column ($\theta_o = 0$) using the current method and the EEM, with the conditions of the latter taken close to their maximum allowed condition of the code. We consider 3 cases of mesh sizes of $(N_1 \times N_2)$ in Eqn. (20): 20x20, 30x30, and 40x40 panels for the HIM and 800 terms for the vertical modes of the EEM. Successive columns of the table corresponds to the normalized surge added mass for increasing values of d/a, at zero frequency. Results for the three mesh sizes, are listed, with errors from the HIM computations compared to the EEM solution, which is highly accurate for the closed slit geometry (h: domain depth/a, K: wave-number). It is clear from this table that the results match quite well. The results compare well for the case of a nonzero slit opening as well, but are not shown here for brevity. For these open-slit cases, the HIM computes much faster than the EEM. Figs. 2 and 3 show the distribution of the jump in the potential (hence the pressure difference on the shell) for the surge and sway motion as indicated in the caption. The slit has a 60-degree opening. The fact that the body acts as a doublet in the far field is clear from the positive pressure on one side and negative on the other. This is not symmetric about the *Oyz* plane because of the nonzero opening. Surging in the direction of the slit lead to a large negative pressure at these sharp edges, where flow separation would be expected in a real fluid. Swaying in the direction normal perpendicular to the slit-opening leads to a solution similar to the closed cylinder. The drop in pressure at the bottom rim of the shell is also evident. Figs. 4 and 5 are plots of the surge and sway added masses as a function of the draft/radius ratio for several slit openings at these limiting frequencies. The coupling added masses $\mu_{12} = \mu_{21}$ are zero by symmetry. Results for added mass in direction $m(=1,2)$ for a body moving in an arbitrary direction β, with respect to the x–axis, can be obtained as a linear combination of the surge and sway results in that direction as follows:

$$\mu_{\beta m} = \mu_{1m}\cos\beta + \mu_{2m}\sin\beta \qquad (21)$$

We note that the added masses (20) approach a fraction of 2 times the mass of the fluid in the cylinder when the draft increases to a large value. The fraction depends on θ_o. The zero-frequency limit solutions approach these limits faster than the infinite-frequency case. In the meeting, the complex behavior of the results with the wave effects *H* in Eqn. (5) will be shown.

5. Acknowledgement. The authors would like to thank Prof. Sergio Sphaier of UFRJ, Brazil, for bringing attention of this design in OMAE-2012. We also acknowledge the American Bureau of Shiping for partial support of this work.

6. References

[1] M. B. A. Moreira, M. Ferreira, and S. H. Sphaier, "Monocolumn hull with internal dock: an alternative for offshore transport of people," in *Proceedings of OMAE 2012*, Rio de Janeiro, Brazil, 2012.

[2] R. W. Yeung, "Added mass and damping of a vertical cylinder in finite-depth waters," *Applied Ocean Research*, vol. 3, no. 3, pp. 119–133, Jul. 1981.

[3] P. A. Martin and F. J. Rizzo, "On Boundary Integral Equations for Crack Problems," *Proceedings of the Royal Society of London. Series A, Mathematical and Physical Sciences*, vol. 421, no. 1861, pp. 341–355, Feb. 1989.

[4] G. Krishnasamy, L. W. Schmerr, T. J. Rudolphi, and F. J. Rizzo, "Hypersingular Boundary Integral Equations: Some Applications in Acoustic and Elastic Wave Scattering," *Journal of Applied Mechanics*, vol. 57, no. 2, p. 404, 1990.

[5] N. F. Parsons and P. A. Martin, "Scattering of water waves by submerged plates using hypersingular integral equations," *Applied Ocean Research*, vol. 14, no. 5, pp. 313–321, 1992.

[6] L. Farina and P. A. Martin, "Scattering of water waves by a submerged disc using a hypersingular integral equation," *Applied Ocean Research*, vol. 20, no. 3, pp. 121–134, Jun. 1998.

[7] P. A. Martin and L. Farina, "Radiation of water waves by a heaving submerged horizontal disc," *Journal of Fluid Mechanics*, vol. 337, pp. 365–379, 1997.

[8] C. J. R. Garrett, "Bottomless harbours," *Journal of Fluid Mechanics*, vol. 43, no. 03, pp. 433–449, 1970.

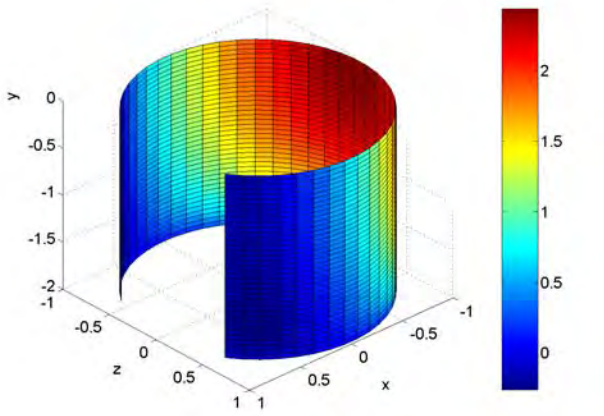

Figure 2: Potential jump over the surface of a surging shell with $d/a = 2, \theta_0 = \pi/6$

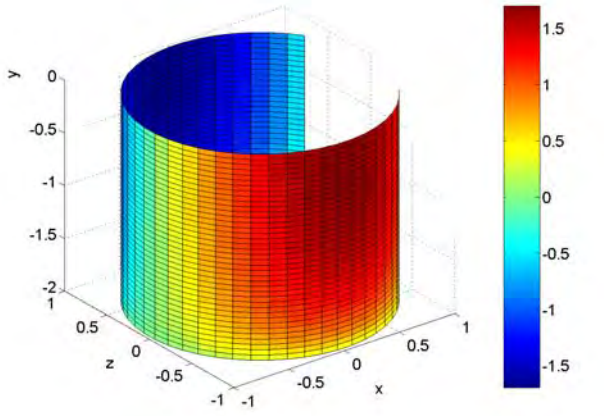

Figure 3: Potential jump over the surface of a swaying shell with $d/a = 2, \theta_0 = \pi/6$

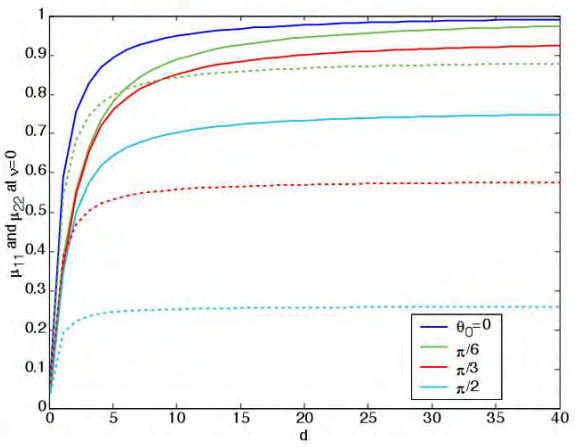

Figure 4: Added mass μ_{11} (solid) and μ_{22} (dashed) at zero frequency versus d/a for various slit opening

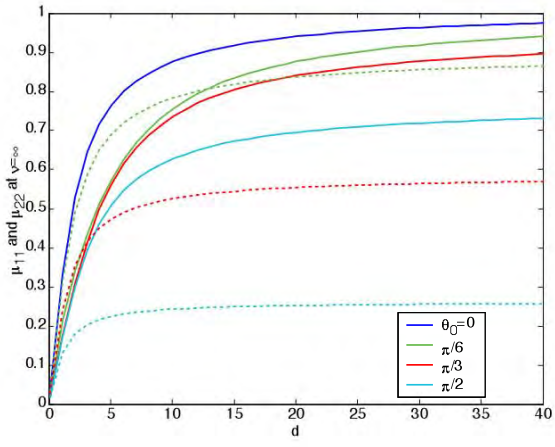

Figure 5: Added mass μ_{11} (solid) and μ_{22} (dashed) at infinite frequency vs. d/a for various slit opening

Table 1: Convergence of the HIM and comparison to EEM for zero-frequency case (see text for details)

d/a	1	2	5	10	20	40
HIM results						
HIM20 (20-20)	0.5680	0.7545	0.9018	0.9571	0.9850	0.9975
HIM30 (30-30)	0.5634	0.7490	0.8959	0.9513	0.9797	0.9935
HIM40 (40-40)	0.5612	0.7464	0.8932	0.9486	0.9772	0.9914
error 20-40* (%)	-1.2195	-1.0821	-0.9636	-0.8909	-0.7928	-0.6151
error 30-40* (%)	-0.3885	-0.3401	-0.3011	-0.2795	-0.2533	-0.2066
EEM results (800-1)	0.5597	0.7396	0.8880	0.9446	0.9721	0.9869
parameters	h=10,K=0.001	h=10,K=0.001	h=20,K=0.001	h=30,K=0.001	h=50,K=0.001	h=100,K=0.001
error HIM20-EEM* (%)	-1.4930	-2.0131	-1.5517	-1.3198	-1.3306	-1.0788
error HIM30-EEM* (%)	-0.6597	-1.2643	-0.8854	-0.7058	-0.7882	-0.6683
error HIM40-EEM* (%)	-0.2702	-0.9210	-0.5825	-0.4251	-0.5335	-0.4608